Supporting Information:

Structural Investigations of Self-Assembled Monolayers for Organic Electronics: Results from X-ray Reflectivity

Artoem Khassanov,[†] Hans-Georg Steinrück,[‡] Thomas Schmaltz,[†] Andreas Magerl,[§] and Marcus Halik[,†]*

[†] Organic Materials & Devices (OMD), Institute of Polymer Materials, Friedrich-Alexander-Universität Erlangen-Nürnberg, Martensstrasse 7, 91058 Erlangen, Germany

[‡] Crystallography and Structural Physics, Friedrich-Alexander-Universität Erlangen-Nürnberg, Staudtstrasse 3, 91058 Erlangen, Germany

[§] Physics Department, Friedrich-Alexander-Universität Erlangen-Nürnberg, Staudtstrasse 3, 91058 Erlangen, Germany

Parameter Confidence Analysis:

In order to gain insight into the confidence analysis and parameter correlations, within the used slab model, in the fits, a Monte Carlo resampling technique[1] was applied, as implemented in Motofit[2]. In this approach, a large number *N* of independent datasets (in our case *N* = 50-500) are randomly synthesized within the actual experimental error bars. The two-four-slab models, as discussed in the manuscript, are subsequently fitted to each of these datasets, resulting in *N* electron density profiles, and *N* parameter sets, respectively. The error bar for each parameter is then derived from the spread of values of that parameter in the *N* data sets. We note that we have chosen to present the best fit parameters, used to calculate the density profile, which in our case are not always the center of the parameter value spread. Such a series of density profiles is exemplary shown for C_{16}-PA/$C_{60}C_{18}$-PA in SI Figure 1, together with the best fit profile (solid red line), indicating the parameter confidence interval.

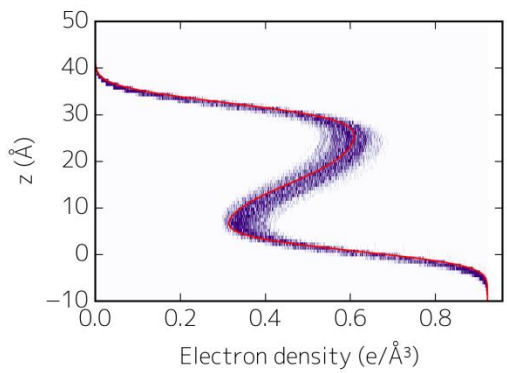

SI Figure 1: Parameter confidence interval analysis for C_{16}-PA/$C_{60}C_{18}$-PA: Electron density profile (solid red line), and parameters confidence interval obtained from a Monte Carlo resampling technique.

A look into the Patterson function:

In order to gather information into the validity of the slab model approach used, we have analyzed the Patterson function[3], which is calculated from Fourier Transformation of the Fresnel-normalized data, using a cosine-window function[2]. The resulting normalized Patterson function *Z(s)*, is exemplary illustrated for C_{10}-PA/$C_{60}C_{18}$-PA and C_{18}-PA/$C_{60}C_{18}$-PA in SI Figure 2, showing peaks for individual and combined real space thicknesses. In the present case, the first peak corresponds to the total monolayer thickness of approximately 33 Å, showing a slight shift (indicated by the solid lines). We note that a similar shift is observed in the model refinement (see SI Table 3). Even though the individual sub-layers cannot be resolved in the

Patterson function, an analysis of different slab models below shows that the high data quality still allows for a resolution of the individual slabs. SI Figure 3 shows the R/R_F of C_{18}-PA/$C_{60}C_{18}$-PA, together with two fits, corresponding to the four-slab fit (solid green line), as discussed in the manuscript, and a three-slab fit (dashed red line), averaging the alkyl chain and head group slab (which could not be resolved by the Patterson function). The three-slab fit describes the general features in the curves, however cannot account for the amplitudes of the larger period Kiessig fringes, likely due to the lack of appreciation of reflection coefficient variations along the molecule. Using the four-slab model, these discrepancies between data and model can however be resolved, resulting in a much improved fit, together with physically meaningful parameters, when considering the molecular geometry.

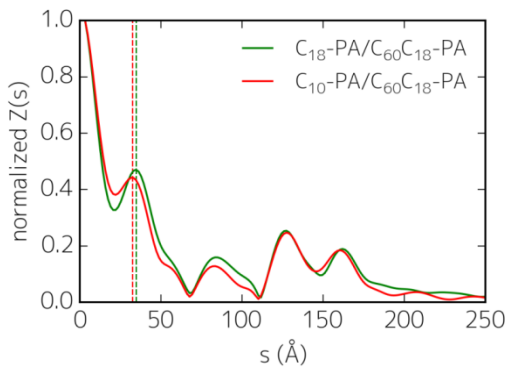

SI Figure 2: Normalized Patterson functions for C_{10}-PA/$C_{60}C_{18}$-PA and C_{18}-PA/$C_{60}C_{18}$-PA showing a shift in the total monolayer thickness (solid lines as guide to the eye).

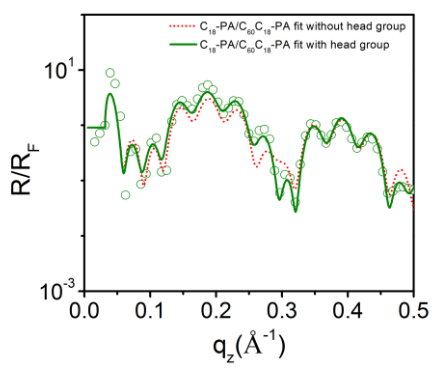

SI Figure 3: R/R_F for C_{18}-PA/$C_{60}C_{18}$-PA and model fits using a single slab averaging alkyl chain and head group (dashed red line) and two separate slabs (solid green line), showing the necessity of the four-slab model discussed in the manuscript.

Effects of spatial resolution:

In an XRR experiment, the spatial resolution is limited due to the limited q_z-range measureable. In this case the electron density and thickness of extremely thin layers can often not be resolved independently and results need to be treated with some caution[4]. However, XRR is still highly sensitive to their product[5–10], which results in a phase-shift, which is necessary to account for in modeling the data, in order to obtain good fits with physically acceptable parameters. In SI Figure 4, the thickness/density pairs of the fitted BTBT-C_{12}-PA anchor slab parameters in the Monte Carlo resampling approach are plotted against each other, indeed showing the discussed correlation (solid line as guide to the eye). However, the majority of points are well within the uncertainties that are given in the manuscript. Further confidence in our model refinement is achieved by considering the large amount of data sets for similar systems, where parameters, such as anchor-group thickness, density and roughness agree well with each other, indicating the robustness in the fits.

Finally, we note that the larger deviations in the low-q_z-range as compared to the high-q_z-range of some data sets, in particular synchrotron data sets, should not be over interpreted in terms of significance of fit-derived parameters values, and can be rationalized when considering the high energy x-rays utilized. This results in extremely low angles, and consequently well-known issues in the low-q_z-range due to e.g. sample over-spill, sample edge effects, and alignment issues.

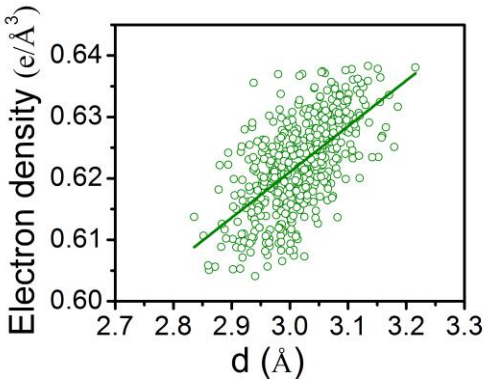

SI Figure 4: Correlation between anchor slab fit parameters, thickness and density, for BTBT-C_{12}-PA, as derived from the Monte Carlo resampling technique, explained in the text.

Discussion of the anchor-group slab:

The thickness of the PA anchor-group slab of ~ 3 Å can be rationalized when considering the molecular geometry and the combined Al-O-P bond length of 3.1 Å. The electron density can be

understood, exemplary for C_{18}-PA, when comparing it to related systems in literature, e.g. silane SAMs on silicon or amphiphilic molecules at liquid surfaces. For example, it is widely accepted that the electron density of a cross-linked silane anchor-group is in the range of 0.50 – 0.71 e/Å^3 [10–12]. When bearing in mind the ratio of the number of electrons in a cross-linked silane anchor-group (30 e^-) and a PA anchor-group (40 e^-) of $\frac{e^-/\text{silane}}{e^-/\text{PA}} \approx 0.75$, the fit-derived values of ~ 0.9 e/Å^3 are reasonable. Furthermore, a similarly enhanced density of the anchor-slab, as compared to the alkyl chain, is found in carboxylic acid monolayers on water, e.g. ~ 0.55 e/Å^3 [13]. Here, the same argument as for the comparison with the silanes SAMs holds, with a ratio of the number of electrons of $\frac{e^-/\text{carboxy}}{e^-/\text{PA}} \approx 0.55$.

Moreover, mass-conservation imposes a similar fit-derived area per alkyl-chain and area per anchor-slab for C_{18}-PA, consistent with our results.

For some systems, e.g. $F_{15}C_{18}$-PA, BTBT-C_{12}-PA and $C_{60}C_{18}$ (pure and mixed) a lower electron density (~ 0.50 – 0.71 e/Å^3) of the anchor-slab is found, as compared to $C_{10\text{-}18}$-PA. This can be rationalized when considering (1) the larger space requirements of the F_{15} and BTBT head-groups, as compared to an alkyl chain, and (2) the significant amount of "touch-down" fullerenes (see Fig. 5 (b), red schematic). Further, for the fullerene SAMs, the electron density of the "alkyl-chain" slab amounts from the combined electron density of the alkyl-spacer (in mixed systems also the C_n-PAs) and the "touch-down" fullerenes. When additionally considering the spatial demands of fullerene moieties in pure and mixed SAMs one can expect a reduced amount of PA anchor groups on the AlO_x surface, consistent with a ~ 45 % reduced fit-derived electron density of the anchor-slab.

Phosphonic Acid Based SAMs on AlO_x:

SI Table 1: Fit-derived parameters of n-alkyl PA (C_{10}-PA, C_{14}-PA, and C_{18}-PA), $F_{15}C_{18}$-PA and BTBT-C_{12}-PA[14] SAMs. Note that the electron densities of the chains (in the case of C_{10}-PA, C_{14}-PA, C_{18}-PA) were constraint to the maximum packing density of hydrocarbon chains in the rotator phase[15]. Bold values correspond to fixed parameters.

		C_{10}-PA	C_{14}-PA	C_{18}-PA	$F_{15}C_{18}$-PA	BTBT-C_{12}-PA
Si	ρ_e ($e/Å^3$)	**0.71**	**0.71**	**0.71**	**0.71**	**0.70**
	σ (Å)	**3.0**	**3.0**	**3.0**	**3.0**	**2.9**
AlO_x	ρ_e ($e/Å^3$)	**0.96**	**0.96**	**0.96**	**0.96**	**0.89**
	d (Å)	$121.2^{+0.1}_{-0.1}$	$122.0^{+0.1}_{-0.1}$	$120.1^{+0.1}_{-0.1}$	$123.3^{+0.2}_{-0.0}$	$123.3^{+0.1}_{-0.3}$
	σ (Å)	**3.0**	**3.0**	**3.0**	**3.0**	$3.9^{+0.1}_{-0.1}$
Anchor	ρ_e ($e/Å^3$)	$0.91^{+0.01}_{-0.01}$	$0.92^{+0.01}_{-0.01}$	$0.93^{+0.01}_{-0.01}$	$0.71^{+0.01}_{-0.01}$	$0.62^{+0.01}_{-0.01}$
	d (Å)	$2.9^{+0.2}_{-0.0}$	$3.0^{+0.1}_{-0.1}$	$2.9^{+0.2}_{-0.0}$	$3.8^{+0.2}_{-0.0}$	$3.0^{+0.3}_{-0.3}$
	σ (Å)	$3.8^{+0.1}_{-0.1}$	$4.3^{+0.1}_{-0.1}$	$3.7^{+0.2}_{-0.4}$	$4.9^{+0.1}_{-0.1}$	$2.3^{+0.2}_{-0.0}$
Alkyl	ρ_e ($e/Å^3$)	$0.32^{+0.01}_{-0.01}$	$0.32^{+0.01}_{-0.01}$	$0.32^{+0.00}_{-0.00}$	$0.27^{+0.01}_{-0.01}$	$0.24^{+0.00}_{-0.01}$
	d (Å)	$11.4^{+0.1}_{-0.1}$	$17.1^{+0.1}_{-0.1}$	$22.9^{+0.1}_{-0.1}$	$8.2^{+0.2}_{-0.0}$	$15.0^{+0.2}_{-0.0}$
	σ (Å)	$2.0^{+0.1}_{-0.1}$	$2.0^{+0.2}_{-0.0}$	$2.3^{+0.2}_{-0.6}$	$4.1^{+0.2}_{-0.0}$	$2.3^{+0.2}_{-0.0}$
Headgroup	ρ_e ($e/Å^3$)				$0.78^{+0.01}_{-0.01}$	$0.48^{+0.02}_{-0.00}$
	d (Å)				$10.0^{+0.2}_{-0.0}$	$7.6^{+0.1}_{-0.3}$
	σ (Å)				$3.1^{+0.1}_{-0.1}$	$3.0^{+0.2}_{-0.0}$

In-Situ XRR on a BTBT-C_{12}-PA System:

An inert (PEEK) coating cell with an integrated substrate with ALD grown AlO_x was filled with a BTBT-C_{12}-PA solution after a reference scan of the substrate/IPA interface had been conducted. The concentration of the SAM solution was diluted to 0.02 mM to extend the time frame, in particular at the beginning of monolayer formation. Further, the duration of one XRR scan was set to approximately 60 seconds, in order to obtain a reasonably precise snap-shot of the SAM condition within a short period of time. In order to minimize radiation damage, each scan was performed at a different spot on the sample. After initial fitting, the parameters of the AlO_x layer were constrained.

SI Table 2: Fit-derived parameters for the in-situ scans during the self-assembly of BTBT-C_{12}-PA SAM. Bold values correspond to fixed parameters. Note that the anchor slab in the reference scan (AlO_x in IPA) was added in order to account for a thin layer adjacent to the substrate. We attribute this to IPA density variations at the interface.

		AlO_x in IPA	30 s	2 min	5 min	10 min	20 min	41 min	103 min	537 min
Si	ρ_e (e/Å^3)	**0.71**	**0.71**	**0.71**	**0.71**	**0.71**	**0.71**	**0.71**	**0.71**	**0.71**
	σ (Å)	**3.0**	**3.0**	**3.0**	**3.0**	**2.9**	**2.9**	**2.9**	**2.9**	**2.9**
AlO_x	ρ_e (e/Å^3)	**0.94**	**0.94**	**0.94**	**0.94**	**0.94**	**0.94**	**0.94**	**0.94**	**0.94**
	d (Å)	119.8	119.1	119.0	119.0	119.0	118.3	119.1	119.4	119.4
	σ (Å)	**3.0**	**3.0**	**3.0**	**3.0**	**3.0**	**3.0**	**3.0**	**3.0**	**3.0**
Anchor	ρ_e (e/Å^3)	0.71	0.77	0.71	0.71	0.71	0.68	0.71	0.71	0.71
	d (Å)	3.1	3.7	4.0	4.0	4.0	4.0	3.4	3.2	3.1
	σ (Å)	2.3	2.5	2.6	2.6	2.5	2.5	2.5	2.5	2.5
Alkyl	ρ_e (e/Å^3)		0.23	0.25	0.25	0.27	0.27	0.27	0.28	0.28
	d (Å)		8.6	9.3	8.9	9.3	8.4	10.0	10.5	10.6
	σ (Å)		2.1	1.6	1.8	2.0	2.2	3.4	3.0	3.0
Headgroup	ρ_e (e/Å^3)		0.30	0.35	0.32	0.35	0.35	0.40	0.42	0.43
	d (Å)		3.4	2.4	5.0	5.2	9.8	11.0	10.8	10.5
	σ (Å)		3.0	2.4	1.4	2.7	3.0	2.3	2.0	2.0
IPA	ρ_e (e/Å^3)		**0.27**	**0.27**	**0.27**	**0.27**	**0.27**	**0.27**	**0.27**	**0.27**

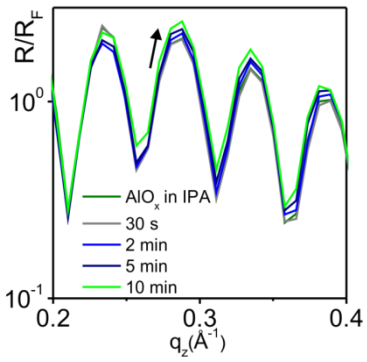

SI Figure 5: Investigation of the self-assembly process of a BTBT-C_{12}-PA SAM on AlO_x. R/R_F data recorded before (substrate in IPA – green) and during the first 10 minutes of the self-assembly of BTBT-C_{12}-PA molecules on AlO_x in IPA (after 30 s - grey; 2 min - blue; 5 min - dark blue; 10 min - lime green). The data range was chosen to highlight the difference of each XRR scan over time, as indicated by the arrow.

Pure and Mixed C_{60}- functionalized SAMs on AlO_x:

Table 3: Fit-derived parameters of pure[16,17] and mixed[17] C_{60} functionalized PA SAMs. For $C_{60}C_6$-PA, a two-slab model was constructed due to the short C_6-alkyl spacer and the observed collapse of C_{60} onto the substrate. Bold values correspond to fixed parameters.

		$C_{60}C_6$-PA	$C_{60}C_{18}$-PA	C_{10}-PA/ $C_{60}C_{18}$-PA	C_{14}-PA/ $C_{60}C_{18}$-PA	C_{16}-PA/ $C_{60}C_{18}$-PA	C_{18}-PA/ $C_{60}C_{18}$-PA
Si	ρ_e (e/Å^3)	**0.71**	**0.70**	**0.70**	**0.70**	**0.70**	**0.70**
	σ (Å)	**3.0**	**2.2**	**2.2**	**2.2**	**2.2**	**2.2**
AlO_x	ρ_e (e/Å^3)	**0.92**	**0.92**	**0.92**	**0.92**	**0.92**	**0.92**
	d (Å)	$103.7^{+0.2}_{-0.4}$	$120.9^{+0.9}_{-0.1}$	$121.1^{+0.4}_{-0.2}$	$119.8^{+0.4}_{-0.0}$	$120.5^{+0.4}_{-0.0}$	$120.1^{+0.5}_{-0.1}$
	σ (Å)	**1.9**	**2.2**	**2.2**	**2.2**	**2.2**	**2.3**
Anchor	ρ_e (e/Å^3)		$0.50^{+0.04}_{-0.01}$	$0.50^{+0.02}_{-0.01}$	$0.50^{+0.01}_{-0.01}$	$0.50^{+0.02}_{-0.01}$	$0.54^{+0.02}_{-0.03}$
	d (Å)		$2.5^{+0.2}_{-0.2}$	$2.5^{+0.2}_{-0.0}$	$2.5^{+0.2}_{-0.0}$	$2.5^{+0.4}_{-0.0}$	$2.5^{+0.0}_{-0.2}$
	σ (Å)		$2.2^{+0.1}_{-0.1}$	$2.2^{+0.5}_{-0.0}$	$2.2^{+0.0}_{-0.0}$	$2.2^{+0.6}_{-0.0}$	$2.2^{+0.1}_{-0.0}$
Alkyl	ρ_e (e/Å^3)		$0.36^{+0.1}_{-0.1}$	$0.30^{+0.01}_{-0.01}$	$0.31^{+0.03}_{-0.02}$	$0.29^{+0.05}_{-0.00}$	$0.30^{+0.01}_{-0.01}$
	d (Å)		$11.6^{+0.8}_{-0.2}$	$11.9^{+0.1}_{-0.5}$	$12.4^{+0.5}_{-0.1}$	$12.7^{+0.5}_{-1.9}$	$14.6^{+0.1}_{-0.3}$
	σ (Å)		$4.0^{+0.5}_{-0.3}$	$3.9^{+0.3}_{-0.3}$	$4.5^{+0.1}_{-0.4}$	$5.2^{+0.5}_{-0.5}$	$6.5^{+0.4}_{-0.2}$
Headgroup	ρ_e (e/Å^3)	$0.56^{+0.01}_{-0.01}$	$0.59^{+0.02}_{-0.04}$	$0.63^{+0.01}_{-0.01}$	$0.63^{+0.01}_{-0.02}$	$0.62^{+0.02}_{-0.05}$	$0.64^{+0.01}_{-0.03}$
	d (Å)	$21.7^{+0.8}_{-0.8}$	$18.2^{+0.1}_{-1.1}$	$17.8^{+0.1}_{-0.6}$	$17.9^{+1.1}_{-0.5}$	$17.4^{+1.3}_{-1.1}$	$15.7^{+0.1}_{-0.3}$
	σ (Å)	$5.7^{+0.1}_{-0.1}$	$2.9^{+0.2}_{-0.2}$	$2.8^{+0.1}_{-0.0}$	$3.1^{+0.1}_{-0.1}$	$2.8^{+0.0}_{-0.2}$	$2.9^{+0.1}_{-0.1}$

SI references:

(1) Heinrich, F.; Ng, T.; Vanderah, D. J.; Shekhar, P.; Mihailescu, M.; Nanda, H.; Lösche, M. A New Lipid Anchor for Sparsely Tethered Bilayer Lipid Membranes †. *Langmuir* **2009**, *25*, 4219–4229.

(2) Nelson, A. Co-Refinement of Multiple-Contrast neutron/X-Ray Reflectivity Data Using MOTOFIT. *J. Appl. Crystallogr.* **2006**, *39*, 273–276.

(3) Tidswell, I.; Ocko, B.; Pershan, P.; Wasserman, S.; Whitesides, G.; Axe, J. X-Ray Specular Reflection Studies of Silicon Coated by Organic Monolayers (alkylsiloxanes). *Phys. Rev. B* **1990**, *41*, 1111–1128.

(4) Uysal, A.; Chu, M.; Stripe, B.; Timalsina, A.; Chattopadhyay, S.; Schlepütz, C. M.; Marks, T. J.; Dutta, P. What X Rays Can Tell Us about the Interfacial Profile of Water near Hydrophobic Surfaces. *Phys. Rev. B* **2013**, *88*, 035431.

(5) Poynor, A.; Hong, L.; Robinson, I. K.; Granick, S.; Zhang, Z.; Fenter, P. A. How Water Meets a Hydrophobic Surface. *Phys. Rev. Lett.* **2006**, *97*, 266101.

(6) Mezger, M.; Sedlmeier, F.; Horinek, D.; Reichert, H.; Pontoni, D.; Dosch, H. On the Origin of the Hydrophobic Water Gap: An X-Ray Reflectivity and MD Simulation Study. *J. Am. Chem. Soc.* **2010**, *132*, 6735–6741.

(7) Mezger, M.; Reichert, H.; Schoder, S.; Okasinski, J.; Schroder, H.; Dosch, H.; Palms, D.; Ralston, J.; Honkimaki, V. High-Resolution in Situ X-Ray Study of the Hydrophobic Gap at the Water-Octadecyl-Trichlorosilane Interface. *Proc. Natl. Acad. Sci.* **2006**, *103*, 18401–18404.

(8) Mezger, M.; Reichert, H.; Ocko, B. M.; Daillant, J.; Dosch, H. Comment on "How Water Meets a Very Hydrophobic Surface." *Phys. Rev. Lett.* **2011**, *107*, 249801.

(9) Ocko, B. M.; Dhinojwala, A.; Daillant, J. Comment on "How Water Meets a Hydrophobic Surface." *Phys. Rev. Lett.* **2008**, *101*, 039601.

(10) Mezger, M.; Schöder, S.; Reichert, H.; Schröder, H.; Okasinski, J.; Honkimäki, V.; Ralston, J.; Bilgram, J.; Roth, R.; Dosch, H. Water and Ice in Contact with Octadecyl-Trichlorosilane Functionalized Surfaces: A High Resolution X-Ray Reflectivity Study. *J. Chem. Phys.* **2008**, *128*, 244705.

(11) Lessel, M.; Bäumchen, O.; Klos, M.; Hähl, H.; Fetzer, R.; Paulus, M.; Seemann, R.; Jacobs, K. Self-Assembled Silane Monolayers: An Efficient Step-by-Step Recipe for High-Quality, Low Energy Surfaces. *Surf. Interface Anal.* **2015**, *47*, 557–564.

(12) Steinrück, H.-G.; Schiener, A.; Schindler, T.; Will, J.; Magerl, A.; Konovalov, O.; Li Destri, G.; Seeck, O. H.; Mezger, M.; Haddad, J.; Deutsch, M.; Checco, A.; Ocko, B. M. Nanoscale Structure of Si/SiO2/Organics Interfaces. *ACS Nano* **2014**.

(13) Als-Nielsen, J.; Jacquemain, D.; Kjaer, K.; Leveiller, F.; Lahav, M.; Leiserowitz, L. Principles and Applications of Grazing Incidence X-Ray and Neutron Scattering from Ordered Molecular Monolayers at the Air-Water Interface. *Phys. Rep.* **1994**, *246*, 251–313.

(14) Schmaltz, T.; Amin, A. Y.; Khassanov, A.; Meyer-Friedrichsen, T.; Steinrück, H. G.; Magerl, A.; Segura, J. J.; Voitchovsky, K.; Stellacci, F.; Halik, M. Low-Voltage Self-Assembled Monolayer Field-Effect Transistors on Flexible Substrates. *Adv. Mater.* **2013**, *25*, 4511–4514.

(15) Ocko, B. M.; Wu, X. Z.; Sirota, E. B.; Sinha, S. K.; Gang, O.; Deutsch, M. Surface Freezing in Chain Molecules: Normal Alkanes. *Phys. Rev. E* **1997**, *55*, 3164–3182.

(16) Khassanov, A.; Schmaltz, T.; Steinrück, H.-G.; Magerl, A.; Hirsch, A.; Halik, M. Interface Engineering of Molecular Charge Storage Dielectric Layers for Organic Thin-Film Memory Transistors. *Adv. Mater. Interfaces* **2014**, n/a – n/a.

(17) Schmaltz, T.; Khassanov, A.; Steinrück, H.-G.; Magerl, A.; Hirsch, A.; Halik, M. Tuning the Molecular Order of C 60 -Based Self-Assembled Monolayers in Field-Effect Transistors. *Nanoscale* **2014**, *6*, 13022–13027.